Observations on the Circulation in the Alboran Sea Using ERS1 Altimetry and Sea Surface Temperature Data

Jorge Vazquez-Cuervo
JPL/Caltech
4800 Oak Grove Dr., M/S 300/323
Pasadena, CA 91109, U.S.A.
jv@pacific.jpl. nasa.gov

Jordi Font
Instituto de Ciencias de] Mar (CSIC)
P. Joan de Borbo
Barcelona 08039, SPAIN
jfont@masagran.uab.es

Juan J. Martinez-Benjamin
Department de Fisica Aplicada
Universitat Politecnica de Catalunya
Campus Nerd - B5
J. Girona Salgado , 31
Barcelona 08034, SPAIN
benjamin@etseccpb.upc.es

08/23/95

Abstract

Data from the altimeter onboard the European Remote Sensing Satellite (ERS 1) was used to study the circulation of the Alboran Sea between -6° to 0° and 35"N to 38°N. This region is dominated by two anticyclonic gyres which are quasi-stationary in space but at times collapse over periods as short as nine days. Maps of sea level residual, between Feb. 1992 and Dec. 1993, were created from the ERS 1 data with high correlation between sea surface temperature and residual sea level in the eastern part of the Alboran Sea. The spatially coherent signal was then extracted using the technique of complex empirical orthogonal analysis with the first 3 modes statistically significant.

The variability of the first CEOF mode appears to be associated with the incoming jet through the straits of Gibraltar with three time periods of high amplitude during the 92-93 time frame. The second and third modes appear to be associated with both the variability of the western and eastern gyre with westward propagation in the third mode evident in the area of the eastern anticyclonic gyre and consistent with previous model results. The results indicate that combining sea surface temperature data and sea level data from altimetry hold promise for understanding the circulation of the Western Mediterranean.

1. Introduction

The Alboran Sea is a small body of water located at the westernmost end of the Mediterranean. Its location at the eastern opening to the Straits of Gibraltar makes it the first basin of the Mediterranean Sea where the water masses associated with Atlantic and Mediterranean characteristics meet, The differences in density between these two water masses, along with the possible changes in potential vorticity due to the flow through the Straits of Gibraltar, make the Alboran Sea an increasingly important area for understanding the dynamics of the Western Mediterranean Basin (example, Gascard and Richez, 1985; Donde Va? Group 1984; Tintore, et al., 1988; La Violette, 1990; Perkins, et al., 1990, Heburn and La Violette, 1990; Perkins et al., 1990).

For the purposes of this study the Alboran Sea will be defined as the area of the Mediterranean between 35°N to 38°N and -6° to O°. This area is dominated by a wave-like front, with two anticyclonic gyres in the western and eastern parts of the basin (Lanoix, 1974; La Violette, 1986; Parrilla and Kinder, 1987; Heburn and La Violette, 1990; Tintore et al., 1991; Viudez et al., 1995; Shirasago et al., 1995). Using hydrographic data, Figure 1 shows the formation of these two gyres in September-October of 1992, while in Figure 2 the two-gyre structure can be seen clearly in the sea surface temperature for the same period of time. In addition the formation of the Algerian Current appears to be tied closely to the dynamics associated with the eastern anticyclonic gyre (Arnone, et al., 1990) also connecting the Alboran Sea to the rest of the western Mediterranean, Heburn and La Violette (1990) examined the temporal variability and identified periods of time when one or the other of the two gyres disappeared completely. Mechanisms for the formation and disappearance. of these two gyres were

examined recently by Speich et al., 1994. They concluded that different factors were responsible for the formation of the western anticyclonic gyre. Conservation of potential vorticity, nonlinearities and the density difference between the two water masses all contributed to the formation of the western anticyclonic gyre. The. gyre itself appeared to be hydro-dynamically unstable with this mechanism given as a possible explanation for the temporal variability observed by Heburn and La Violette (1990). The formation of the anticyclonic gyre in the eastern basin of the Alboran Sea appears correlated with changes in the Almeria-Oran front and the Algerian current (At-none et al. 1990). Heburn and La Violette (1990) determined that a minimum two active-layer reduced gravity model was necessary for the formation of this double-gyre s ystem. The y examined the disappearance and appearance of these gyres in terms of remote forcings due to winds and propagation of events from the western Mediterranean and determined that these mechanisms must be taken into account when exan ining the temporal variability of the two-gyre structure. Observations of the temporal variability of the two gyres will be examined in this paper. Because of cloud cover in the satellite infrared data, resolving the temporal and spatial scales from this data set is problematic (Heburn and La Violette, 1 990).

This study will attempt to combine sea surface height data from the European Remote Sensing Satellite (ERS1) altimeter with sea surface temperature data taken from the NOAA series of advanced high resolution radiometers (AVHRR) to analyze the possible temporal variability and spatial variability of the two gyres and the circulation in the Alboran Sea. Emphasis will be placed on establishing the usefulness of combining sea surface temperature and altimetric sea level data in studying the circulation in the Alboran Sea and its temporal variability. The purpose of the paper is to use these two data sets to examine the space-time structure of the circulation as well as possible

periodicities associated with the appearance and disappearance of the western and eastern anticyclonic gyres in the Alboran Sea. If successful, the use of ERS 1 and TOPEX/Poseidon altimetric data can be applied to the entire Western Mediterranean. Specifically the sea surface temperature will be used to qualitatively validate the altimeter data and the appearance and disappearance of the gyres. Once the altimetric data are validated qualitatively, a set of complex empirical orthogonal functions (CEOF) will be derived to separate the variability into spatially coherent modes and examine the spatial and temporal scales.

2. Altimeter Data and Processing

To examine the space-time variability in the Alboran Sea, altimeter data from the European Remote Sensing Satellite (ERS 1) were extracted in an area between 35°N to 38°N and -6°to 0° (see Figure 3). Orbit characteristics of the satellite were such that the satellite repeated its ground track every 35 days with the altimeter sampling along-track every 7 kilometers during the period between April 14, 1992 and December 15, 1993 (Battrick, 1993). Data from February of 1992 to April 14 were used during which the satellite was in the three-day repeat. The mission was carried out predominately in the 35-day repeat (Vass and Handoll, 1991), during which the spacing of the ground tracks between 35-40°N was approximately 60 kilometers. Standard processing procedures commonly used with altimeter data were applied to the ERS 1 data (Zlotnicki, 1989(a)) set in the given area. Such procedures include the application of environmental corrections and blunder removal techniques, geoid removal, removal of orbit error, and removal of the tides. The ERS 1 IGDR data were received from NOAA.

To remove the geoid and time independent part of the sea surface height, a mean surface from Rapp (1991) was interpolated to the along-track position and subtracted from the sea surface height. A bi -cubic spline was used to do the interpolation. At a given along-track grid position, points were removed which were more than five standard deviations away at the given grid location. To remove tides in the area, a Mediterranean tide model (Canceill et al., 1994) was interpolated in space-time. to the given along-track positions of the ERS 1 altimeter. This model contains eight tidal components which include the solid earth and ocean tides.

The usual procedure for removing orbit error over a regional area the size of the Mediterranean is to remove a quadratic over arc lengths of 1000-2000 km (see Zlotnicki et al., 1989a). On these scales it has been shown that the orbit error behaves as a quadratic trend in the along-track direction. Initially ERS 1 data were extracted in an area between -10° to 0° and 20° to 60° N. After removal of the geoid, a quadratic was removed in the along-track direction from each pass in the given area. It was determined that the residual sea level standard deviation on the order of 80 centimeters was too large to be due to oceanographic changes and that residual orbit error was still a problem. A similar procedure to remove orbit error was attempted again, but instead of removing a quadratic over an arc between 20° to 60° only that part of the arc that crossed the Mediterranean was used. In addition a linear tilt and bias were removed instead of a quadratic to minimize removing any possible oceanographic signal. Residual sea level values after geoid removal were now approximately 20-30 centimeters, and on the order of oceanographic variability for the given area. Thus, the proper application of techniques to remove the orbit error is critical, even in inland seas such as the Mediterranean where the length of orbit tracks may be on the order of a few degrees. The problem of applying orbit correction techniques over gaps in orbit tracks has been observed and documented in previous studies (see Zlotnicki et al., 1989a and Zlotnicki, 1989b).

In order to obtain maps of sea surface height, an iterative successive correction technique (Bratseth, 1986) was applied to interpolate the residuals of sea level to a regular series of maps in time and space. The technique has been applied successfully in previous studies using altimetric data (Vazquez et al., 1990). In the. area between -6° to 0° and 35°N to 38”N, the along-track values of residual sea level were interpolated to a regular grid in space-time based on the following equation:

$$F_x^a(v+1)=F_x^a(v) + \sum_{i=1}^{n} w_{xi}(v)(F_i^o(v)-F_i^a(v))/\sum_{i=1}^{n} w_{xi}(v) \qquad (1)$$

where $F_x^a(v)$ is the interpolated (analyzed) value at position x, iteration v; $F_i^o(v)$ is an observed value at position i; and $F_i^a(v)$ is the estimate of $F_i^o(v)$ from the vth iteration. The weighting factors, $w_{xi}(v)$, are now a function of space and time where the time weight is based on a Gaussian function and the spatial part uses a Cressman weighting (Vazquez et al., 1990). Weights were determined from data sampling characteristics and typical scales of variability for the given area. For each iteration "v" the weighting factors decrease in order to force the interpolated values to converge to the data values. Three iterations were chosen based on a best fit of the data to the interpolated values. For the first iteration the spatial correlation scale of 100km was based upon the distance between neighboring tracks. The value of 100km corresponds also to the approximate scale of the anticyclonic gyres. This value was reduced to approximately 60km for the second iteration and 40km for the third iteration. The corresponding e-folding time scales were 35, 34, and 33 days, respectively. The time scales for the study area include at least one full repeat of the ERS 1 altimeter. The successive correction interpolation was applied to data in the area between -6° to 00 longitude and 35°N to 38°N latitude from February 4, 1992 to Dec. 15, 1993 where maps of sea level residual were created every ten days with a spatial grid resolution of 8 points per degree of latitude and longitude. In order to include data from the last possible date of Dec. 15, while taking into account the 35-day e-folding time scale, it was decided to run the interpolation up through April of 1994. Thus, the interpolation was carried out for 80 maps but only 73 of these maps of sea level had data, However, because the ERS 1 altimeter had a repeat cycle of 35 days, maps created every ten days are not independent. These 73 maps formed the database for the analysis of the observations of the circulation in the Alboran Sea using complex

empirical orthogonal function analysis (CEOF). The addition of the seven maps with values of O had no effect on the calculation of the CEOF modes because the FFT computation in the CEOF code requires a cosine tapering. Adding the seven maps changed only the bandwidth in the CEOF calculation and provided the equivalence of tapering the data while making sure all the data were used in the calculation.

3. Sea Surface Temperature Data and Correlations with Altimeter Observation

In order to qualitatively validate the results from the sea level residuals derived from the ERS 1 altimeter, comparisons were made with data from the NOAA 11 multi-channel advanced resolution radiometer which measures sea surface temperature (MCSST). This satellite was part of a series of NOAA satellites launched with radiometers to measure sea surface temperature (SST). The multi-channel configuration allows for correction for water vapor and clouds (McClain, et al., 1985). Because changes in circulation in the Alboran Sea are associated with changes in both sea surface temperature and dynamic height, these two parameters should be correlated in time. The two anticyclonic gyres have a clear signature in infrared imagery (e. g., Heburn and La Violette, 1990) and should display significant changes in sea surface height across their associated geostrophic jet, MCSST data were available for 1992 and overlapped with the first year of the ERS 1 mission. The purpose of this validation was to see if the altimeter data were accurately representing the disappearance and appearance of the two anticyclonic gyres.

Because the resolutions of the sea level grids as derived from the ERS 1 altimeter are different from the MCSST data, it was necessary to interpolate and bin the MCSST data in space and time so that the two grids matched. Then a correlation coefficient in time could be calculated at each spatial grid location. The initial resolution of the sea surface temperature data consisted of weekly composites at a resolution of 18 kilometers. To match the sea level grids, it was necessary to bin the weekly composites into ten-day bins and interpolate the 18-kilometer data to an 8 point/degree spacing between 35”N to 38°N and -6° to O^{o}. The interpolation was done using a routine from

the Interactive Data Language (IDL) called min_curve_surf. IDL is a commercial software package that includes both visualization and mathematical routines for use with scientific data sets. The algorithm used is based on fitting a minimum curvature spline surface to the data points. This algorithm was selected over a hi-cubic spline because of the irregularity, due to cloud cover, of the sea surface temperature data. The result of the binning and interpolation were a series of sea surface temperature maps at the same temporal and spatial resolution as the residual sea level maps. For 1992, 35 maps of sea surface temperature could be correlated directly with identical maps of residual sea level.

Figure 4 shows the spatial correlation for the area of the Alboran Sea between sea surface temperature and residual sea level. Values ranged from a minimum of -0.6 to a maximum of 0.8. To estimate the 95% level of confidence, 12 degrees of freedom were used. Based on the weekly composites there are values of sea surface temperature every seven days, but the 35-day repeat of the ERS 1 altimeter allows, on the average, only one independent measurement every month, Thus, 12 degrees of freedom is based on the repeat cycle of the ERS 1 altimeter. Using 12 degrees of freedom, all correlations higher than 0.57 and lower than -0.57 will be significant at the 95% level. In the area of the eastern anticyclonic gyre values are statistically significant. Apparently highs in correlation are associated with the area of the eastern anticyclonic gyre, the formation of the Algerian Current, and frontal zones where the signature in both sea level and sea surface temperature would be largest. Nonetheless, the significant correlations with sea surface temperature indicate that qualitatively the sea level and temperature are correlated in areas of expected high variability associated with the formation of the eastern anticyclonic gyre and the Algerian current.

In addition Figure 4 indicates an area of low correlation that should be associated with variability due to the Western anticyclonic gyre. Due to cloud cover, part of the reason for the low correlations in this area could be due to the inherent gaps found in the sea surface temperature data. These gaps are seen in Figure 5 which show the distribution of data on a weekly basis at six different grid locations in the Alboran Sea. If the data were perfect, there should be one point per bin for the 52 weeks. However, significant times are clearly visible where data are missing. At longitude -4.8°, latitude 35.8° no data are available between approximately week 20 and week 37 of 1992. If the Western gyre either appeared or disappeared during this period of time, it would not be seen in the sea surface temperature record. At longitude -4.8°, latitude 36.0° a significant gap occurs between week 18 and week 30 of 1992. At the other four locations the data were distributed more evenly indicating less possibility of missing events associated with gyre formation. This same type of behavior was found in other locations in the Alboran Sea. Thus, it is quite probable that in the area of the Western anticyclonic gyre, cloud cover is preventing the observations of the formation or collapse of this gyre.

Figure 6 is a map showing the standard deviation in centimeters of sea level in the Alboran Sea for the 1992-1993 time period. Highs in variability occur in areas commonly associated with the formation and collapse of the two anticyclonic gyres. Maximum values range from around 30 centimeters in areas associated with the Western anticyclonic gyre to 15-20 centimeters in areas associated with the formation of the eastern anticyclonic gyre and Algerian current. However, in some areas of poor correlation (see Figure 4), values of high variability are identified clearly. It appears that gyre formation or collapse is taking place during this period, but is clearly being missed by the sea surface temperature data. The usefulness of using altimetric data to

study the circulation patterns in the Alboran Sea becomes apparent as persistent cloud cover in the AVHRR data for a given area can lead to erroneous conclusions about the appearance and disappearance of the gyres. To separate the variability into a set of dominant and spatially coherent modes, the technique of complex empirical orthogonal analysis was applied.

4. CEOF Methodology

Because the technique of complex empirical orthogonal functions has been applied in previous studies in meteorology and oceanography (see Lorenz, 1956; Vazquez, 1993), only a brief synopsis will be given here. For more details on this technique see Horel (1984).

Due to the inherent noisiness of satellite data, a technique such as the CEOF approach that can extract the dominant signal, can prove useful. The technique has proven successful especially in situations when there is an idea about the physical phenomena being identified. For example, in the Gulf Stream (Vazquez, 1993) it proved successful in identifying a large-scale 2000km westward propagating feature. This feature had been predicted by thin-jet models (Cushman-Roisin, 1993). In applying this technique to the Alboran Sea, it was hoped to extract the signals dealing with the variability of the two anticyclonic gyres.

The technique of CEOF analysis is similar to real EOFS in that the variability is separated into a set of spatially uncorrelated and orthogonal modes. However, CEOF's have the added advantage that they can detect propagating features while real EOF's can be used to detect only stationary or standing waves. To replicate propagating features from the real EOF analysis the *mocks* must be summed together, an arbitrary method of separating the variability. From Vazquez (1993), the procedure is similar to real EOFS in that one calculates a spatial covariance matrix at each grid point (x,y) where x and y are now grid locations referring to some latitude and longitude coordinate. The time series at each point (x,y) is now complex where the real part of the time series corresponds to the actual data values and the imaginary part is the 1 lilbert transform of the real part.

Mathematically this can be expressed for a given grid point (x,y) as a complex time series where:

$$H_p(x,y,t)=H_r(x,y,t) + H_i(x,y,t) \quad (2)$$

and $H_r(x,y,t)$ are the data values at the given grid location (x,y) for a time "t". $H_i(x,y,t)$ is the Hilbert transform or simply the real part $H_r(x,y,t)$ shifted by 90°. The Hilbert transform may be calculated by using the Fourier coefficients derived from the actual data values. The rest of the procedure is identical to the case of real EOF's except that the spatial covariance matrix is now complex. Because the spatial covariance matrix is hermitian the eigenvalues are real and represent the percent variability explained by a given mode. The eigenvectors are complex and are associated with a real and an imaginary part. The eigenmode may be represented by a temporal phase and amplitude and a spatial phase and amplitude. The slope of the temporal phase is a measure of the instantaneous frequency while the two-dimensional gradient of the spatial phase is a measure of the wavelength in the "x" and "y" direction. For further details on the CEOF approach see Vazquez et al., (1993). The four parameters temporal phase and amplitude, and spatial phase and amplitude will be examined to determine the space-time scales of the significant modes of sea level residual in the Alboran Sea.

5. Results

As described previously, the technique of complex empirical orthogonal analysis separates the variability in the given area into modes which are uncorrelated and orthogonal to each other. Figure 7 indicates that the first three modes account for 45%, 18% and 7% of the data, respectively. Together these modes account for approximately 70% of the variability. The analysis was cut off at the third mode because not only does the modal structure become rapidly degenerate but the phase and amplitude structures of the modes become increasingly difficult to interpret due. to additional noise in their structure. To verify that these first three modes were at the 99% level of confidence a monte-carlo technique was applied to the region (Overland and Preisendorfer, 1982). For each of the grid points in the Alboran Sea a Gaussian random number generator in time with a standard deviation of 25 units was applied. Seventy-three maps were produced for the area of the Alboran Sea and run through the CEOF program. This procedure was repeated 100 times with all eigenvalues explaining greater than 0.5 percent of the variance stored. This process led to 3957 eigenvalues for the 100 runs of the CEOF analysis. Figure 8 is a histogram of the 3957 eigenvalues, indicating that no eigenvalue greater than 5 was found. This is consistent 'with the fourth CEOF mode explaining approximate y 6% of the variability and approaching the noise level. Thus, these first three modes were examined to determine the spatial and temporal scales of variability as well as to compare with previous results in the area.

Figures 9(a,b) are the temporal amplitude and phase for the first CEOF. Three maxima in the amplitude of this mode occur at approximately day 150 of 1992, 110 of 1993 and 335

of 1993. The first two peaks occur in the Spring of 1992 and 1993, with the third peak occurring in the late Fall of 1993. Thus, this mode appears to be associated with an almost annual cycle in 1992, shifting to a different periodicity in 1993. This behavior is identified clearly from the temporal phase where the slope of the phase vs. time (frequency) suggests an annual cycle is dominant for 1992 while the slope changes dramatically during 1993, This change indicates that the first mode is not periodic during the two-year analysis period of the data set.

Figures 10(a,b) show the spatial structure of the first CEOF. This CEOF has a high between -5° and -4° degrees longitude and 35°N and 36° N. A maximum in variability exists further north at the same longitude between 36° N and 37°N. A local maximum exists also between -2° and -10 and 35"N and 36° N although its magnitude is much less than the one between -5° and -4°. The spatial structure of this mode appears to indicate that a large percentage of the variability is associated with the formation and collapse of the western anticyclonic gyre. The ability of the CEOF technique to extract spatially coherent signals within a larger domain is exemplified, Figure 10b indicates that the phase in the area of the westernmost maximum is constant. The constant phase is consistent with a stationary wave pattern. However, there is a 180° phase difference between the highs in the northern and southern part of the Western Alboran Sea. The maximum found in the eastern basin of the Alboran Sea is associated with a phase which is not constant and changes in an almost east-west pattern, indicating propagation in that direction. However spatially the phase is meaningful only at those locations where there is a high in amplitude. Figures 11 (a,b) are plots of the temporal amplitude and phase for the second CEOF. Figure 11a indicates that a maximum in the temporal amplitude occurs in the Spring of 1992 with secondary maxima in the winter of 1992-93 and summer of 1993. The general trend of the CEOF appears to be one where the amplitude

decreases in 1993. The peak in the Spring of 1992 coincides with an identical peak in the first CEOF. The amplitude changes of this CEOF indicate that a large percentage of the variability y of this CEOF occurs from January of 1992 through July of 1993. The slope of the plot of temporal phase versus time indicates a constant frequency of 2-3 cycles/year for the two-year period of the record.

Plots of the spatial structure of the second CEOF are shown in Figures 12(a,b). The spatial amplitude of this mode show several distinct highs. One *occurs* between -5° and -4° at approximately 36°N. Other highs occur between -2° and -1" at 35.5°N and 36°N; -().5° and 37°N and -0.5° and 37.5°N. Thus, the spatial structure of this mode appears more complicated than that of the first CEOF. The spatial phase shown in Figure 12b indicates that the spatial maximum found between -5° and -4° behaves in an almost stationary wavelike pattern, a conclusion based on the constant phase found in the given area, The phase structure is more complicated with the highs in the eastern Alboran Sea. The lines of constant phase occurring in the eastern basin, and perpendicular to the coast, are significant because of the high amplitudes found in the region, unlike the spatial phase of the first CEOF.

Figures 13(a,b) are the plots showing the temporal structure of the third CEOF. The general trend of increasing amplitude toward the middle of 1993 to the beginning of 1994 is opposite that of the first CEOF. A maximum in this CEOF occurs at day 600 or the summer of 1993. Other secondary peaks occur during the Spring of 1993 and Fall of 1993. The maximum amplitude of these peaks appears to be on the order of 10 to 20 centimeters. The slope of the temporal phase found in Figure 13(b) appears to indicate that during 1993 the frequency of this mode was approximately 2-3 cycles/year. It

appears that 1992 was associated with an almost annual period. As with the first CEOF mode the frequency of this mode appears to change between 1992 and 1993.

Figures 14(a,b) show the spatial structure of the third CEOF. Outside the Alboran basin there is a high at 37.5°N with five other maxima appearing in the structure of this CEOF. Highs are visible at approximately (-4°, 35.5°N); (-4 °,36.5°N); (-1.5°, 35.6°N); (-2.7°, 35.5°N); and (-2°, 36.8°N). The spatial pattern of this CEOF is indicative of the complexity of this structure. Figure 14(b) shows that the spatial phase of this mode is similar to the first CEOF. The two highs in the western part of the basin are approximately 180° out of phase. This same structure is found also in the first CEOF where the two highs in the western part of the basin are 180° out of phase. The phase contours, or lines of constant phase for this mode, are north-south in the western part of the basin, indicating some of type of southwest or northwest propagation.

6. Discussion

Results from the CEOF analysis indicate that Alboran Sea circulation is varying in both time and space. Previous results (Heburn and La Violette, 1990) indicate that both the western and eastern gyms are highly variable in time and quasistationary. As a first step it was important to determine if the spatial and temporal resolution of the ERS 1 altimeter were sufficient to resolve the scales of variability of the first CEOF mode, which is most likely associated with the variability of the western anticyclonic gyre. To accomplish this, a simple model was applied in the western basin of the Alboran Sea using the spatial and temporal structure of the gym..

a. Simulation

The spatial structure of the first CEOF indicates that there is a high at approximately 35.7°N, -4.5° and 36.4°N, -4.4°. To reproduce the spatial structure of these gyres , a Gaussian was applied centered at each of these locations. Two Gaussians were generated for each maximum such that:

$$f_1(r) = \exp - \frac{(r\text{-}al)z}{2b^2}$$

and

$$f_2(r) = \exp - \frac{(r\text{-}a_2)^2}{2b^2}$$

where al (x,y) and a_2(x,y) represent the centers of the Gaussians at positions (x,y) or (35.7°N, -4.5°and 36.4°N, -4.40). "b" is the standard deviation of the spatial scale and was chosen to be 20 kilometers to realistically represent the spatial scale of the western

gyre. The 20km standard deviation represents approximately the 100km extent of the anticyclonic gyres found in the Alboran Sea (e.g., Heburn and La Violette, 1990; Speich et al., 1995; Tintore et al., 199 1) where $r(x,y)$ is the position from the center of the Gaussian. Thus, $(r(x,y)-a(x,y))^2$ represents the distance from the center of the two Gaussians. To determine the effect of both Gaussians, the two functions were summed, or for a given longitude, latitude point (x,y), the simulated spatial function becomes:

$$f(r) = f_1(r) + f_2(r)$$

However these gyres vary also in time thus the temporal variation was modeled as a sine function with a given frequency and amplitude. The temporally varying part of the simulated data were generated using:

$$A(t)=A_{max}\sin(\omega t)$$

where

w was chosen to be 1.5 cycles/year and

A_{max} was 38 centimeters. The frequency and amplitude were chosen to represent the characteristic frequency and amplitude found in the first mode. In addition a spatial phase difference of 180° between $f_1(r)$, $f_2(r)$ was applied to simulate the phase difference found in the first CEOF. The function $g(r,t)=f(r)*A(t)$ was then calculated for each grid point (x,y) and time (t). Values of longitude and latitude (x,y) and time (t) *were* taken directly from the ERS 1 geophysical data record. Values of $g(r,t)$ were then

run through the successive correction routine to generate the maps of simulated data at the same temporal and spatial resolution as the maps of sea level residual. As before, a set of CEOF was derived based on the 73 maps of sin related data. The first CEOF was found to account for over 80% of the variance indicating that due to inadequate sampling, etc., there might be some leakage of the signal into the second mode. Figures 15(a,b) show the spatial amplitude and phase of the first simulated CEOF. Maxima occur at the approximate geographical locations associated with $a_1(x,y)$ and $a_2(x,y)$. In addition the spatial phase of the simulated data clearly show the 180 degree phase difference between $a_1(x,y)$ and $a_2(x,y)$. East of -3°' the phase, as expected, becomes increasingly noisy as one gets farther from the center of the Gaussians. Although not shown, the temporal amplitude and phase are consistent with a maximum amplitude of 38 units and a frequency of 1.5 cycles/year. Thus, the simulation has shown that the ground track spatial and temporal coverage of the ERS 1 altimeter is sufficient to resolve the spatial scale of the western anticyclonic gyre, along with cycles close to the annual period. Because the scale of the eastern anticyclonic gyre s similar to the western gyre, the coverage provided by the ERS1 altimeter should be sufficient to resolve both gyres.

b. Comparison with previous results and models

In general, using the approach of separating the variability in a data set into uncorrelated and orthogonal modes has proved successful in studies where one hopes to retrieve a known signal. A major reason for the intial focus of this study in the Alboran Sea was because of its large known signal in both sea level and sea surface temperature, thus making it easier to interpret and accurately assess the feasibility of using the CEOF approach for larger basin-scale studies. Modeling and observational studies of

the Alboran Sea (Heburn and La Violette, 1990 and Speich, et al., 1995) indicate that three different gyre-scale circulation patterns can exist in the Alboran Sea:

1) the Western gyre is present but the Eastern gyre is absent

2) the Western gyre is absent is but the Eastern gyre is present

3) both the Western and Eastern gyres are present.

One would expect the results from the CEOF analysis to be reflective of these circulation patterns. One advantage of the CEOF analysis over conventional EOF analysis is the ability to [differentiate regional patterns of coherence (Vazquez, 1993). It has the ability to filter things which are episodic and periodic in nature. These two properties are important in the Alboran Sea where it is not known if the formation of the two gyres are correlated. In addition Heburn and La Violette (1990) showed that the temporal variability of the two gyres is more episodic than periodic. Thus, the CEOF approach lends itself to the dynamics of the area.

The location of the two maxima in the first CEOF indicate that the variability in the first CEOF is likely to be associated with changes in the incoming jet or even the Western anticyclonic gyre. However, the two maxima are out of phase (see Figure 10(b)) indicating that if the circulation associated with the southern maximum is anticyclonic, the circulation of the northern maximum is cyclonic. This scenario is consistent with model results (Speich, et al., 1995) which indicate the in phase formation of a cyclonic eddy just north of the main anticyclonic gyre. It is consistent with observations of cyclonic eddies north of the main anticyclonic gyre (see La

Violette, 1984; Parilla and Kinder, 1987; Tintore et al., 1991; Viudez et al., 1995). The formation of the cyclonic eddies at the same time as the anticyclonic western gyre is consistent with their appearance in the same CEOF. Thus, these two features must be spatially coherent.

The variability in the second CEOF appears to be associated with a high in the area of the Western anticyclonic gyre; in addition highs are visible at (36.80,-0.50), (35.3°, -1.5), (36°, -1°) and (37.8°, -0.50). The high at (37.8°, -0.5°) is a persistent feature in all three CEOF's, but because it is on the boundary of the study area, its interpretation in terms of some dynamics in the Alboran Sea is difficult. The maximum at (35.3°, -1 .5°) is approximately at the location of the coastal jet which forms following the collapse of the Eastern gyre. From the spatial phase (Figure 12) this maximum is 180° out of phase with the maximum at (36°, -10, which is approximately at the location of the Algerian Current. The significance of this spatial amplitude and phase structure indicates that the formation of the coastal current following the collapse of the Eastern gyre does not coincide with the formation of the Algerian Current. Another explanation is the formation of a cyclonic circulation at (36°, -1°) coinciding with the anticyclonic circulation at (35.3°, -1 .50). This explanation is consistent with the appearance of the Algerian current at approximately (36°, - 1°) during the formation of the eastern anti-cyclonic gyre. Although the high at (36.8°,-0.50) might be associated with the formation of the Almeria-Oran front one usually associates the Almeria-Oran front with a maximum found between -2° and O^{o}. Once again this maximum is close to the boundary of the study area which could lead to problems of interpretation if its formation is associated with events outside of the Alboran Sea. Nonetheless, the maxima at (36.8°,-0.50) and (37.8°, -0.5°) could be associated with variability due to

the interaction between the Mediterranean water, which flows to the southwest along the Spanish coast, and the eastern Alboran gyre that can give rise to the formation of the Almeria-Oran front and the generation of the Algerian current east of 10. These correlations between the Algerian Current, the collapse of the Eastern gyre, and the formation of the Almeria-Oran front and coastal current would be consistent with previous results (Tintore et al., 1988). However, the results must be interpreted with caution due to the limited size of the study area.

The spatial structure of the third CEOF (Figure 14(a,b)) seems clearly associated with changes in the structure of the eastern and western anticyclonic gyres. The spatial phase of this mode is interesting in that it is the only mode where one of the maxima is associated with propagation. The spatial phase of the western anticyclonic gyre indicates little or no propagation but its formation represents a quasi-stationary pattern, consistent with earlier results. The phase contours for the maximum located at the position of the eastern anticyclonic gyre change across the maximum indicating a propagation along the African coast. Because the phase contours from the CEOF analysis are relative, to determine the direction of propagation one must examine the time series for that particular mode. An animation of the third CEOF indicates that the direction of propagation along the African coast is westward. This type of scenario where the westward displacement of the eastern Alboran gyre causes the disappearance of the western anticyclonic gyre is consistent with reduced-gravity model results (Heburn and La Violette, 1990) where the baroclinicity of the model increases with the strength of the undercurrent. When the inflow of the bottom layer is greater than the upper layer, the meanders from the Algerian Basin propagate into the Alboran Sea, causing the displacement of the eastern gyre and the eventual disappearance of the western gyre.

Although the temporal components of the first three CEOF's indicate an almost episodic formation and disappearance of the gyres and their associated structures these results must be interpreted with caution. The appearance of the gyres *in* the Alboran Sea can take place rapidly (Heburn and La Violette, 1990), on time scales as short as nine days. Thus, the repeat orbit of the ERS 1 altimeter (35 clays) is not sufficient to resolve completely the temporal scales of motion and in certain instances may miss entirely an event associated with the appearance or disappearance of one of these gyres. Nonetheless, the first CEOF is dominated by three large amplitude events, occurring over different times of the year for the 1992-1993 time frame. The second CEOF appears to be dominated by a large event during the summer of 1992. The third CEOF has an increase in the amplitude during the 1993 time frame. If these results are indicative of the temporal changes in the gyres of the Alboran Sea, their behavior is not likely to be dominated by seasonal changes in the wind stress or other forcing on the annual time scale.

7. Conclusions and Summary

Combining sea level data from the ERS 1 altimeter and sea surface temperature data derived from the NOAA polar orbiting multi-channel advanced high resolution radiometer has proved an effective step toward using satellite data in studying the temporal and spatial changes of the circulation in the Alboran Sea. The circulation in this region is dominated by two anticyclonic gyres which at times disappear completely (Heburn and La Violette, 1990). To extract the spatially coherent and long-period signal in the region, a set of complex empirical orthogonal functions was derived. After applying a monte-carlo simulation it was determined that the first three modes were significant at the 99% level of confidence.

All three modes are associated with spatial maxima in the areas of the western and eastern anticyclonic gyres. In addition, a comparison with sea surface temperature data indicate significant correlations in areas associated with the eastern anticyclonic gyre and the Almeria-Oran front. However, low correlations exist in areas associated with the western anticyclonic. This was determined to be due to a lack of sea surface temperature data because of cloud cover in the region. The 30cm to 40cm signal is consistent with previous results in the area (Tintoré et al., 1991). The phase difference between the two dominant maxima found in the first mode is consistent with model results which show the formation of a cyclonic gyre north of the inlet to the Straits of Gibraltar and which is also associated with the formation of the western anticyclonic gyre (Speich, et al., 1995). The second CEOF appears to be associated with the variability of the Almeria-Oran front and perhaps the formation of the Algerian current. The third mode is associated with a

westward propagating feature in the area of the eastern anticyclonic gyre. This feature is correlated with the formation of a quasi-stationary feature in the area of the western anticyclonic gyre.

The results in this paper indicate that both sea surface temperature and sea level data derived from satellites hold tremendous promise in terms of *their* ability to understand the circulation of the Western Mediterranean. However, a problem in using sea surface temperature is persistent cloud cover . Only the altimeter can provide a continuous time series over a long period of time. In an area such as the Alboran Sea where the circulation can change over a period of a few days due to the appearance and disappearance of the two anticyclonic gyres, the 35-day repeat orbit of the ERS 1 altimeter is not sufficient to resolve the temporal variability of these features. Thus, future satellite studies of the area need to include a combination of sea surface temperature and in-situ data to fully *resolve* the temporal variability of these features. Results from this study hold promise for assimilating maps of sea level residual into circulation models of the area. This appears essential to predict the than ges in the gyre scale circulation of the Alboran Sea. As a next step in this research, the study area should be expanded to include the entire Western Mediterranean Basin.

Acknowledgments

The authors would like to thank Olaf Gnade for his assistance in processing the ERS 1 altimeter data. John Lillibridge is thanked for his diligence in sending out periodic updates regarding the ERS 1 processing. Patrick Vincent at CNES sent the original tide model that was applied to remove the tidal constituents in the Alboran Sea. Bernardo Shirasago provided the ATSR image for comparison purposes. The research began while Jorge Vazquez-Cuervo was a visiting scientist at the Institute of Marine Science in Barcelona, Spain. The Project on Space Research ESP93-0879-C02-02 from the Spanish Commission for Science and Technology (CICYT) is gratefully acknowledged for financial assistance. The study is a contribution to ESA Earth Observation Program (ERS-1 AO El project) and to the EUROMODEL- MTP EC MAST Program (contract MAS2-CT93-O066). The Spanish CICYT gave economic support to the research through project AMB93-1372-CE. J. Vazquez-Cuervo was a visiting scientist at ICM Barcelona in 1993 funded by the Spanish Ministerio de Educacion y Ciencia (grant SB92-A337 10418). The Centre de Supercomputacio de Catalunya provided computing resources. ERS - 1 altimeter data were provided by ESA. Currently J. Vazquez-Cuervo is under contract with the National Aeronautics and Space Administration at the Jet Propulsion Laboratory where the research was completed and the manuscript prepared.

References

Arnone, R. , D. Wiesenburg and K. Saunders, 1990: The origin and characteristics of the Algerian Current, *J. Geophys. Res.*, **95,** (C2), **1587-1598.**

Battrick, B. , 1993: *ERS1 User Handbook,* ESA Publications Division ESTEC, Noordwijk, The Netherlands, 128pp.

Canceill, P., P. Agelou and P. Vincent, 1995: Barotropic tides in the Mediterranean Sea using a finite element model, *J. Geophys. Res.*, in press.

Cushman-Roisin, B., L. Pratt and E. Ralph, 1990: A general theory for equivalent barotropic thin jets, *J. Phys. Oceanogr.*, *23,91-103.*

Donde Va? Group, 1984: (Donde Va?) An oceanographic experiment in the Alboran Sea, The oceanographic report, *EOS Trans. AGU, 65,682-683.*

Gascard, J. C. and C. Richez, 1985: Water masses and circulation in the western Alboran Sea, and in the Straits of Gibraltar, *Progress in Oceanography, 15, 157-216.*

Heburn, G. W. and P. E. La Violette, 1990: Variations in the structure of the anticyclonic gyres found in the Alboran Sea, *J. Geophys. Res., 95,* (C2), *1599-1613.*

Horel, J. P., 1984: Complex principal component analysis: Theory and examples, *J. Clim. Appl. Meterol.*, *23, 1660-1673.*

Lanoix, F., 1974: Project Alboran, Etude hydrologique et dynamique de la Mer d' Alboran, *Tech. Rep. 66,* NATO, Brussels,71 pp.

La Violette, P.E., 1986: Short term measurements of surface currents associated with the Alboran Sea during (Donde Va?), *J. Phys. Oceanogr.*, *16,262-279.*

La Violette, P. E., 1990: The Western Mediterranean Circulation Experiment (WMCE): Introduction, *J. Geophys. Res.*, *95, 1511-1514.*

Lorenz, E, N., 1956: Empirical orthogonal functions and statistical weather prediction, *Rep. 1*, 49 pp., Stat. Forecasting Proj., Mass. Inst. of Technol., Cambridge, Mass.

McClain, E. P., W. G. Pichel and C. C. Walton, 1985: Comparative performance of AVHRR-based multichannel sea surface temperature, *J. Geophys. Res.*, 90, C6, 11587-11601.

Overland, J. E., and R. W. Presiendorfer, 1982: A significance test for principal components applied to a cyclone climatology, *Mon. Weather Rev.*, **110,** 1-4.

Parilla, G., T. H. Kinder, 1987: The physical oceanography of the Alboran Sea, Naval Ocean Research and Development Activity, Report 184,26 pp.

Perkins, H., T. H. Kinder, and P. E. La Violette, 1990: The Atlantic inflow in the western Alboran Sea, *J. Phys. Oceanogr.*, *20, 242-2.63.*

Rapp, R. H., Y.-M, Wang and N.K. Pavlis, 1991: *The Ohio State 1991 Geopotential and Sea Surface Topography Harmonic Coefficient Models Report 410,* Dept. Geodetic Science and Surv., The Ohio State Univ., Columbus, Ohio 43210-1247.

Shirasago, B., E. Garcia Gorriz and J. Font, 1995 (in press) : Comparison between ERS-1 SAR images Acoustic Doppler Current Profiler (ADCP) velocity data in the Alboran Sea, *Proceedings of the European Symposium on Satellite Remote Sensing,* Rome, Italy.

Speich, S., G. Madec and M. Crepon, 1995: The circulation in the Alboran Sea: a sensitivity y study, submitted to *J. Phys. Oceanogr.*.

Tintoré, J. D., P. E. La Violette, I. Blade and A. Cruzado, 1988: A study of an intense density front in the eastern Alboran Sea: the Almeria-Oran Front, *J. Phys. Oceanogr.*, *18, 1384-1397.*

Tintoré, J. D., J. D. Gomis, S. Alonso and G. Parrilla, 1991: Mesoscale dynamics and vertical motion in the Alboran Sea, *J. Phys. Oceanogr.*, *21, 811-823.*

Vass, P. and M. Handoll, 1991: *UK ERS-1 Reference Manual,* Royal Aerospace Establishment, Famborough, UK., 131 pp.

Vazquez, J., 1993: Observations on the long-period variability of the Gulf Stream downstream of Cape Hatteras, *J. Geophys. Res.,* 98, (Cl 1), 20133-20147.

Vazquez, J., Zlotnicki, and L.-L. Fu, 1990: Sea level variabilities in the Gulf Stream Cape Hatteras and 50° W: A Geosat study, *J. Geophys. Res.*, 95, C(10), 17957-17964.

Viudez, A., J. Tintore and R. L. Haney, 1995: Three-dimensional structure of the two anticyclonic gyres in the Alboran Sea, *J. Phys. Oceanogr.* (accepted).

Zlotnicki, V., A. Hayashi, and L.-L. Fu, 1989a: The JPL-OCEANS-8902 version of the Geosat altimetry data, *JPL Intern. Dec. D-6939, 47* pp., Jet Propul. Lab., Pasadena, CA..

Zlotnicki, V., L.-L. Fu, and W. C. Patzert, 1989b: Seasonal variability in global sea level observed with Geosat altimetry, *J. Geophys. Res.*, 94, C(I 2), 17959-17969.

Figure Captions

1. The Alboran Sea in the Western Mediterranean. The dynamic topography of the 10 dbar surface referenced to 230 dbar shows the structure of the two anticyclonic gyres in October 1992 (campaign from the EUROMODEL group, see Viudez et al., 1995).

2. Sea surface temperature of the Alboran Sea on the 28 September 1992, as recorded by the Along Track Scanning Radiometer of the ERS-1 satellite with 1 km resolution in the horizontal (from Shirasago et al., 1995).

3. ERS 1 altimeter ground track locations in Alboran Sea. Anomalous track found between -3° and -2° occurred when the ERS 1 satellite was in a three-day repeat orbit at the beginning of the mission and during the start of 1994. Otherwise, ground tracks are associated with the predominant 35-day repeat orbit.

4. Spatial plot of temporal correlation between sea surface temperature and sea level residual in the Alboran Sea. After interpolation spatial grid resolution is 8 points per degree of latitude and longitude. Contour interval 0.1.

5, Distribution of cloud free sea surface temperature images in the Alboran Sea at four different grid locations. Values of" 1" on the y-axis indicate sea surface temperature was available for that week while values of "O" indicate no value of sea surface temperature was available for that week. Plot labels indicate longitude and latitude.

6. Spatial plot of standard deviation in centimeters of sea level residual for the Alboran Sea fortwo-year period. After interpolation spatial resolution is 8 points per degree of latitude and longitude. Contour interval is 5 centimeters.

7. Percent variability explained by the first 10 empirical orthogonal modes vs. mode number.

8. Distribution of eigenvalues for CEOF modes for 100 runs using a Gaussian random number generator to generate values with a standard deviation of 25 units.

9. (a) Temporal amplitude for the first CEOF mode. For purposes of plotting temporal amplitude is multiplied by the total number of grid points. Time axis is in days from January 1, 1992.

(b) Temporal phase for the first CEOF mode.

10. (a) Spatial amplitude for the first CEOF mode. For purposes of plotting the spatial amplitude is divided by the total number of grid points. Contour interval is 0.5.

(b) Spatial phase for the first CEOF mode. Contour interval is 60 degrees.

11. (a) Temporal amplitude for the second CEOF mode. For purposes of plotting temporal amplitude is multiplied by the total number of grid points. Time axis is in days from January 1, 1992.

(b) Temporal phase for the second CEOF mode

12. (a) Spatial amplitude for the second CEOF mode. For purposes of plotting the spatial amplitude is divided by the total number of grid points. Contour interval is 0.5.

(b) Spatial phase for the second CEOF mode. Contour interval is 60 degrees.

13. (a) Temporal amplitude for the third CEOF mode. For purposes of plotting temporal amplitude is multiplied by the total number of grid points. Time axis is in days from January 1, 1992.

(b) Temporal phase for the third CEOF mode

14. (a) Spatial amplitude for the third CEOF mode. For purposes of plotting the spatial amplitude is divided by the total number of grid points. Contour interval is 0.5.

(b) Spatial phase for the third CEOF mode. Contour interval is 60 degrees.

15. (a) Spatial amplitude for the first CEOF mode derived from the simulated data set based on the generation of Gaussians at two different spatial locations in the Alboran Sea. Location of the center of the Gaussians were at (35.7°N, -4.5° and 36.4”N, -4.40).

(b) Spatial phase for first simulated CEOF

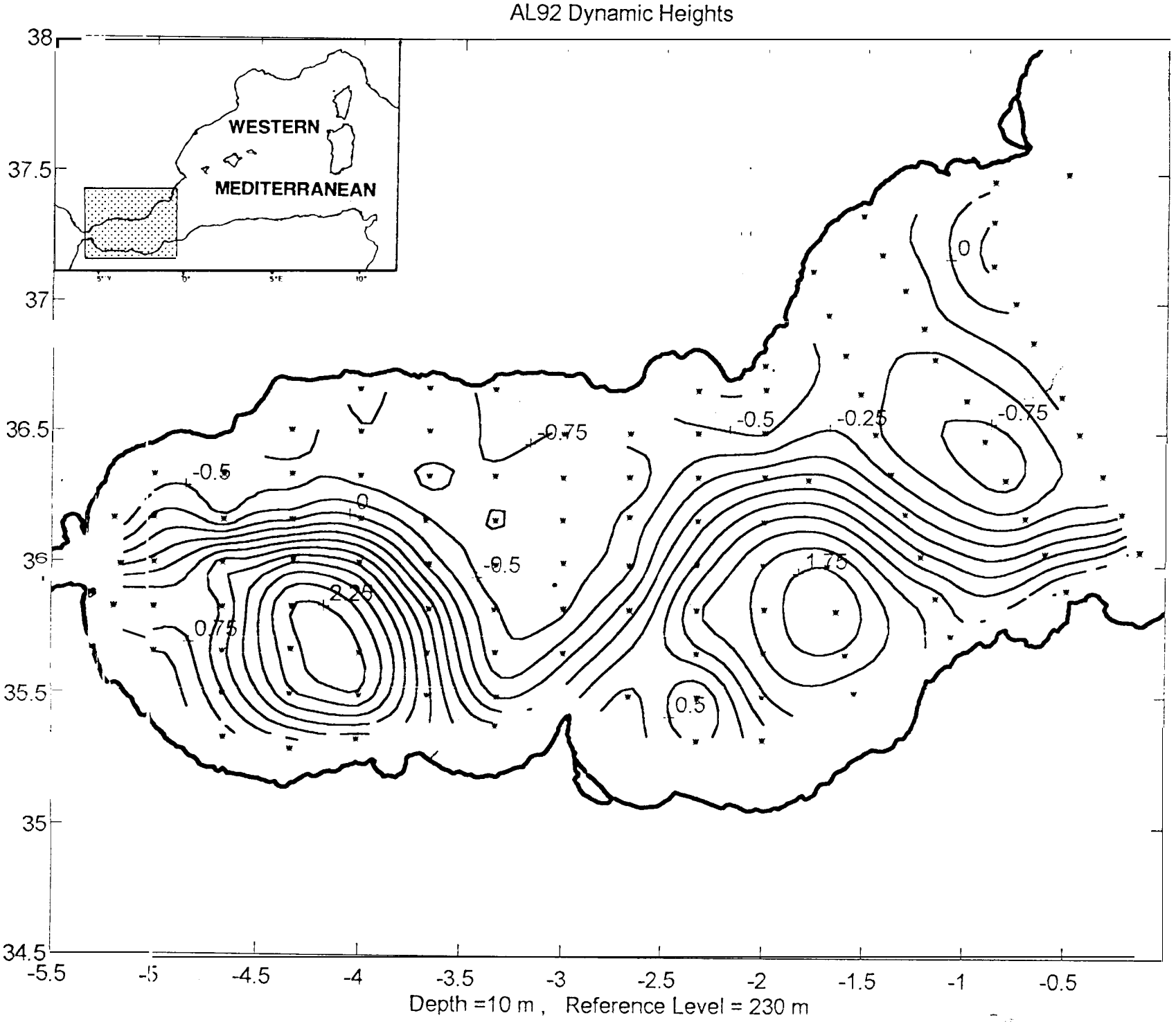
AL92 Dynamic Heights
WESTERN
MEDITERRANEAN
38
37.5
37
36.5
36
35.5
35
34.5
-5.5
-5
-4.5
-4
-3.5
-3
-2.5
-2
-1.5
-1
-0.5
0
-0.5
-0.75
-0.5
-0.25
-0.75
-0.5
0
-0.5
2.25
0.75
1.75
0.5
Depth =10 m , Reference Level = 230 m

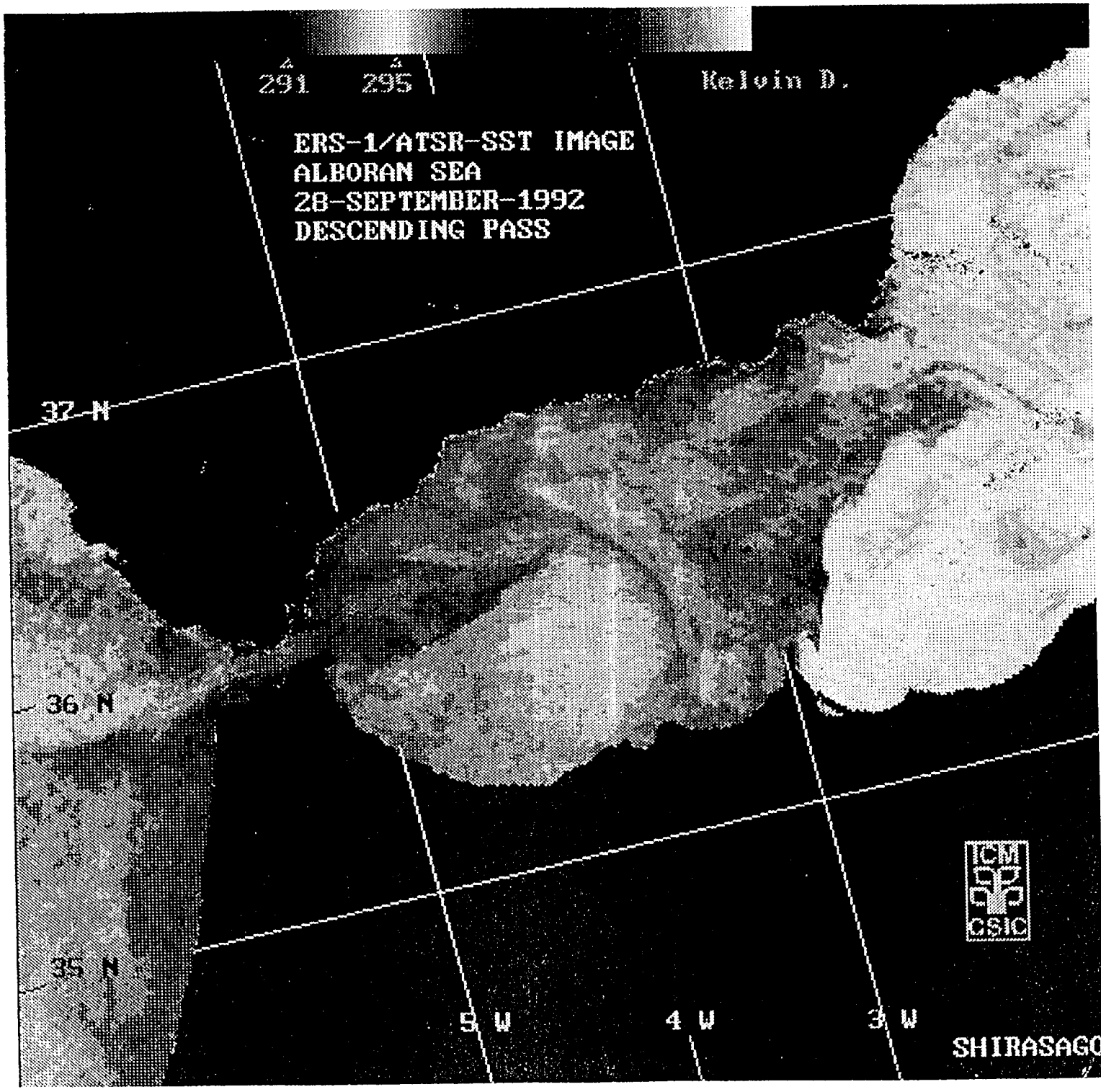
291 295
Kelvin D.
ERS-1/ATSR-SST IMAGE
ALBORAN SEA
28-SEPTEMBER-1992
DESCENDING PASS
32 N
36 N
35 N
5 W
4 W
3 W
ICM
CSIC
SHIRASAGO

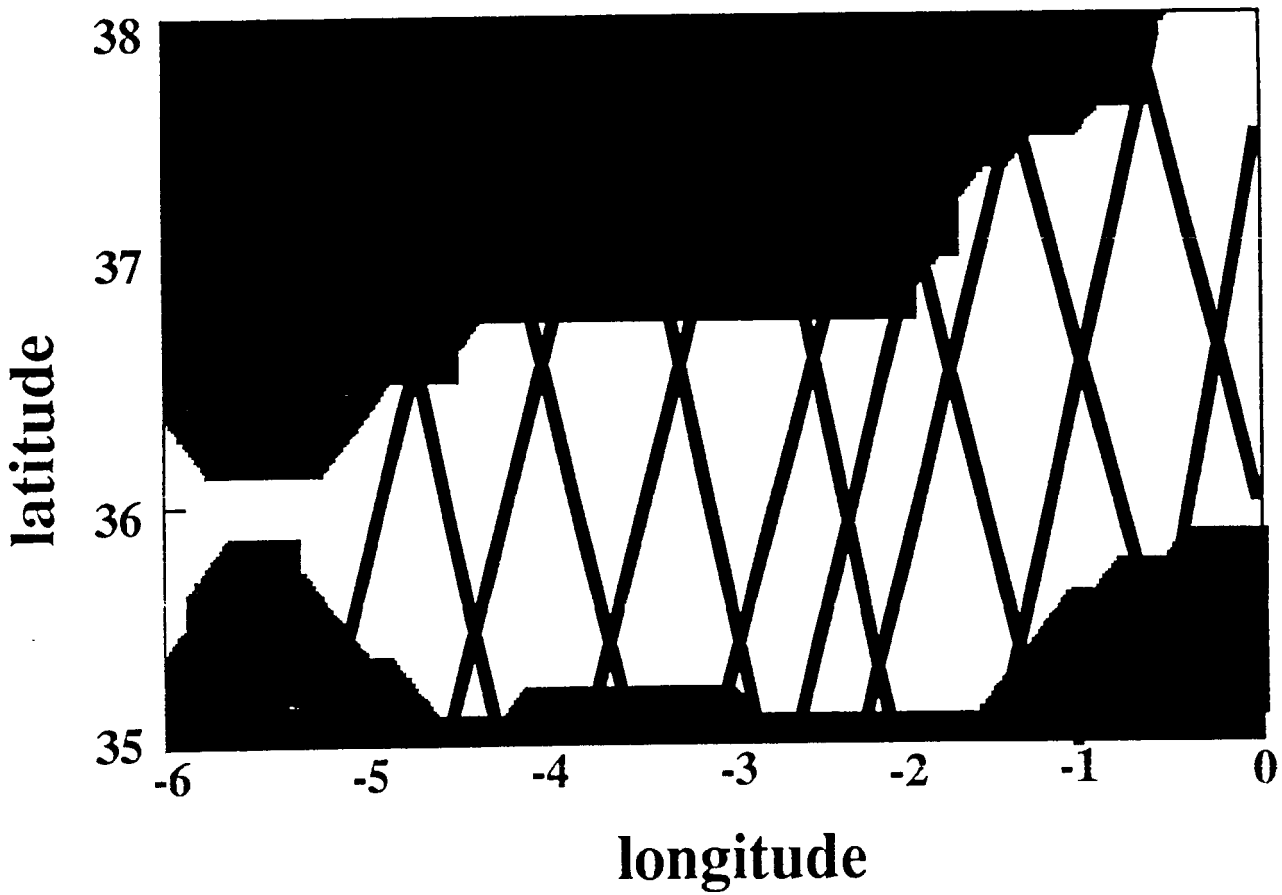
38
37
36
35
latitude
-6
-5
-4
-3
-2
-1
0
longitude

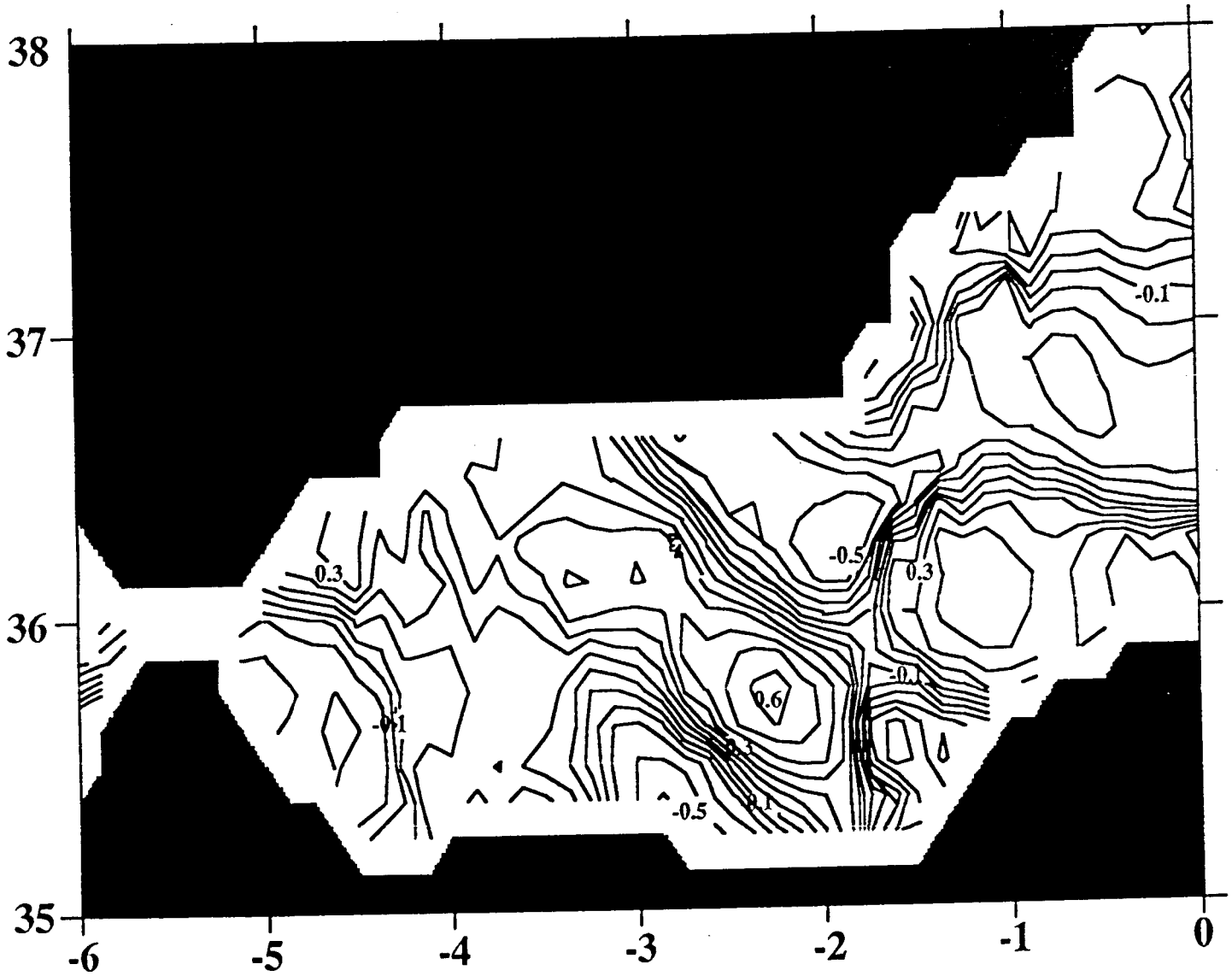
38
37
36
35
-6
-5
-4
-3
-2
-1
0
-0.1
0.3
-0.5
0.3
-0.1
0.6
-0.1
-0.5
0.1

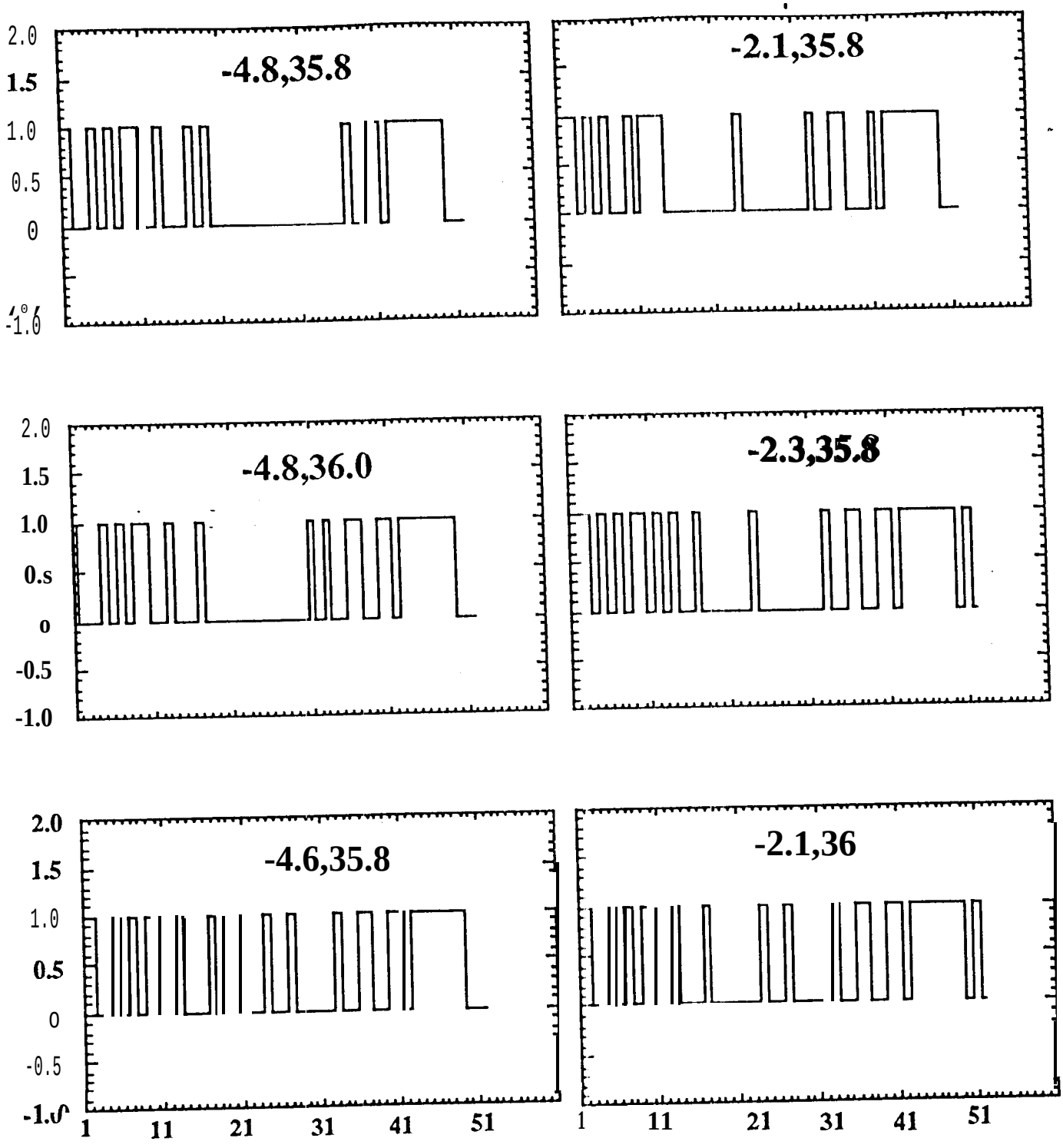
-4.8,35.8
-2.1,35.8
-4.8,36.0
-2.3,35.8
-4.6,35.8
-2.1,36
2.0
1.5
1.0
0.5
0
-0.5
-1.0
1
11
21
31
41
51
number of points per weekly bin
weeks from Jan. 1st 1992

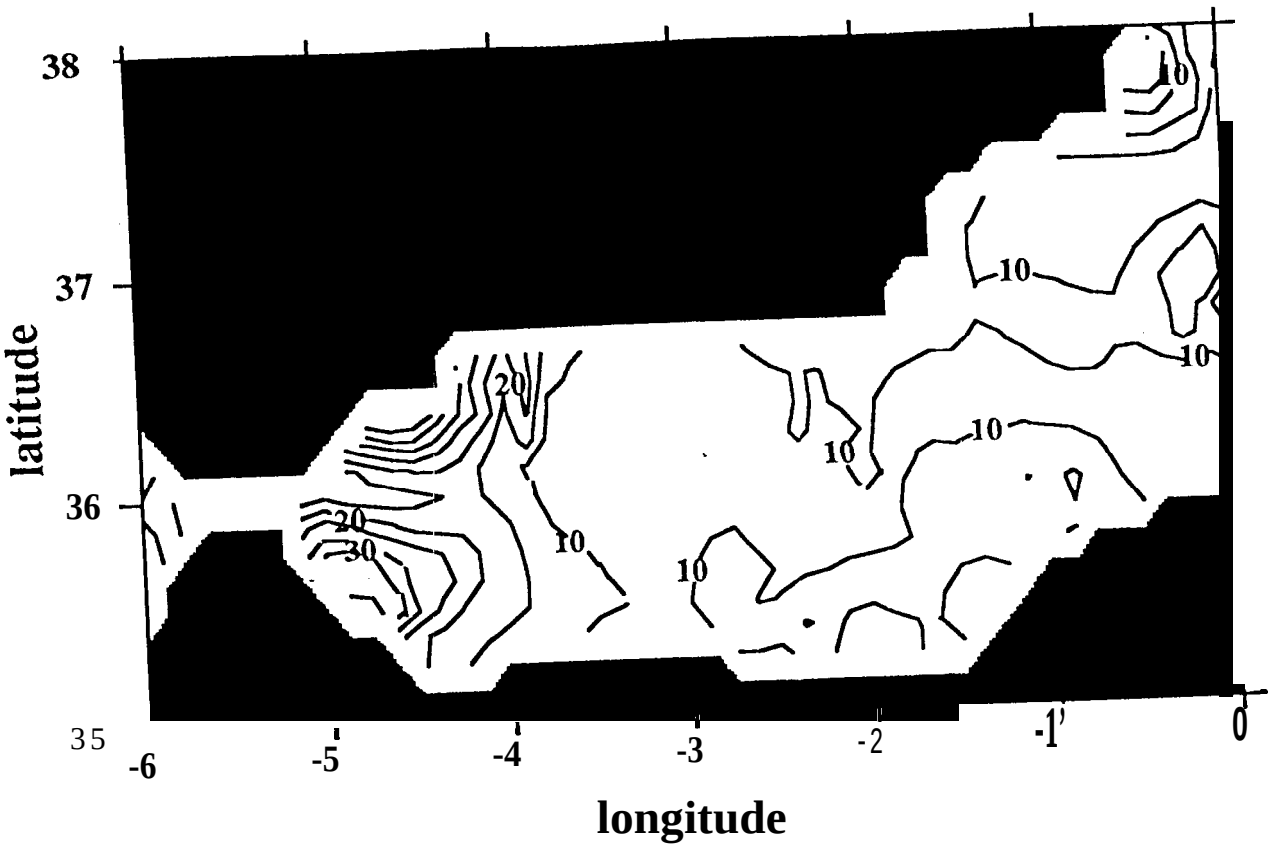
38
37
36
35
latitude
-6
-5
-4
-3
-2
-1
0
longitude
10
10
10
10
10
10
20
20
30

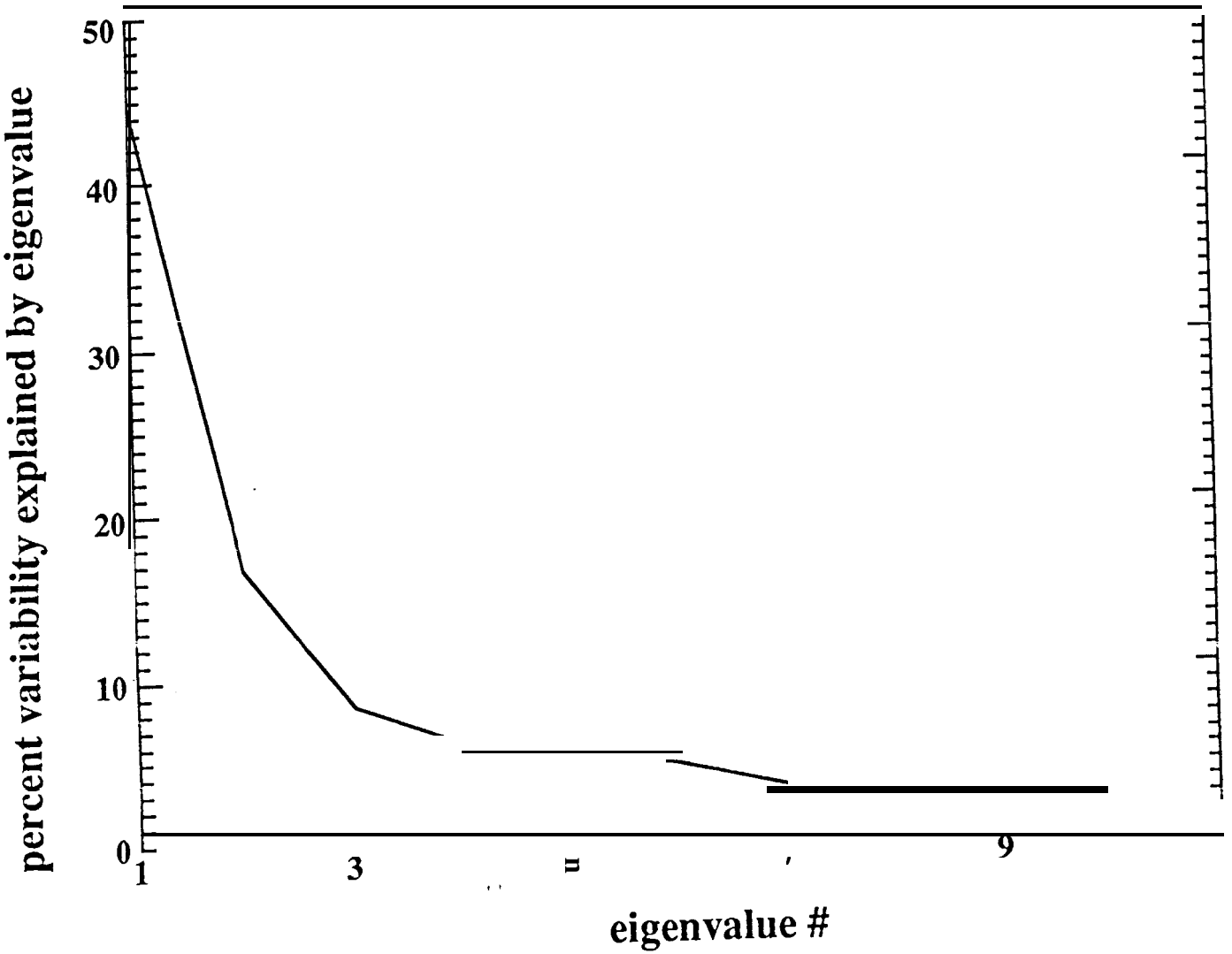
percent variability explained by eigenvalue
50
40
30
20
10
0
1
3
9
eigenvalue #

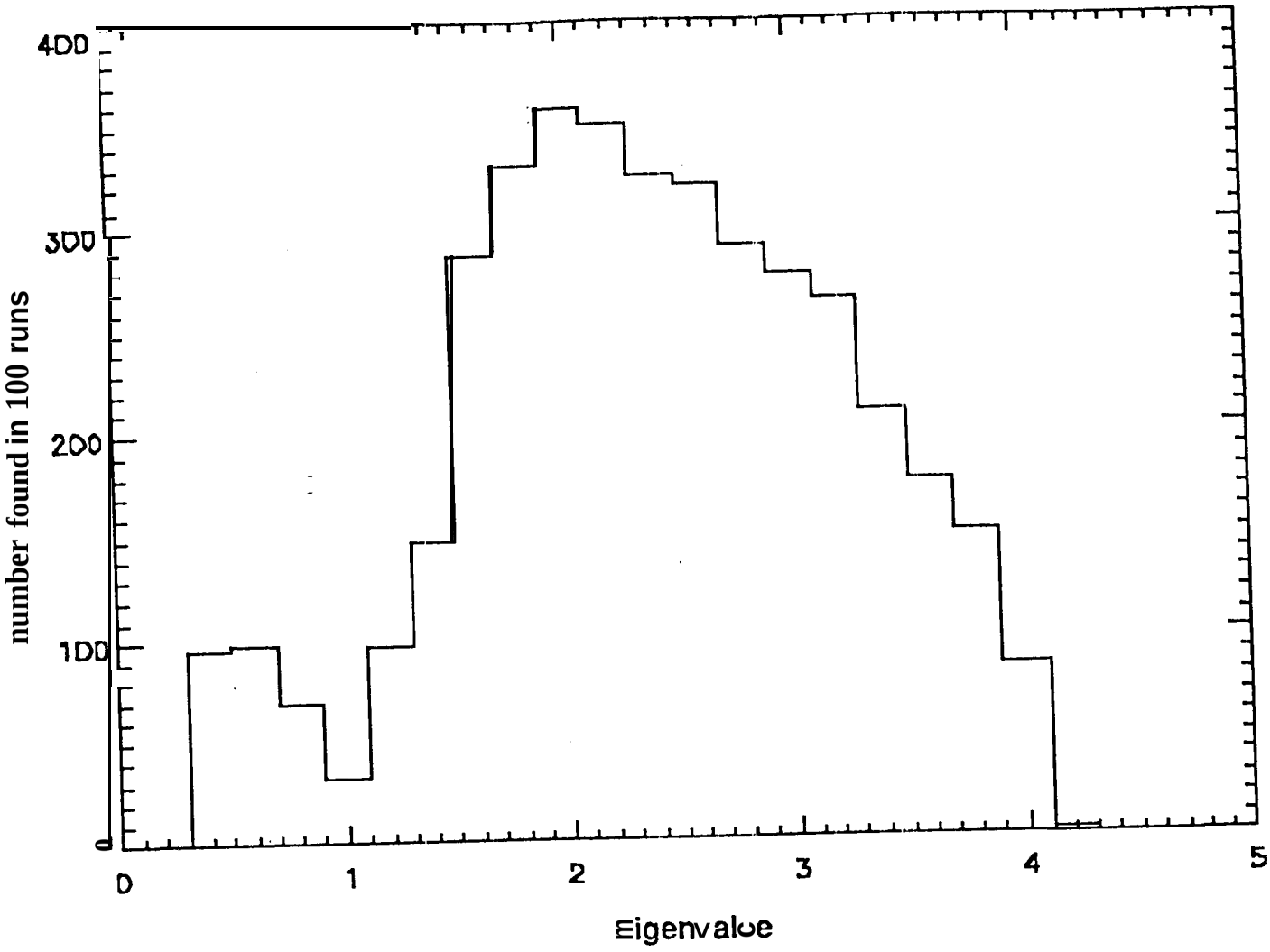
400
300
200
100
0
number found in 100 runs
0
1
2
3
4
5
Eigenvalue

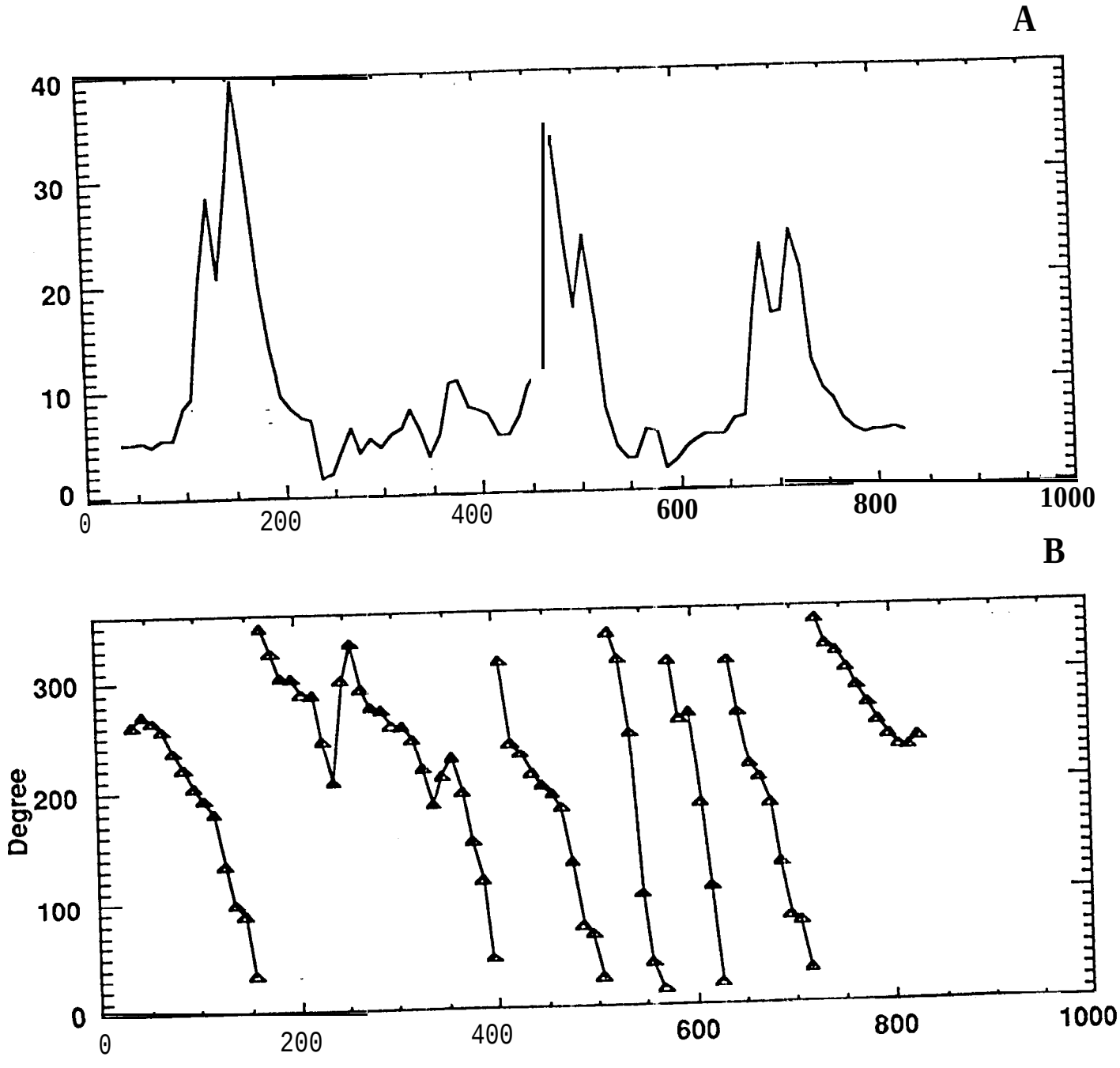
A
40
30
20
10
0
0
200
400
600
800
1000
B
Degree
300
200
100
0
0
200
400
600
800
1000
Time in days from 1/1/92

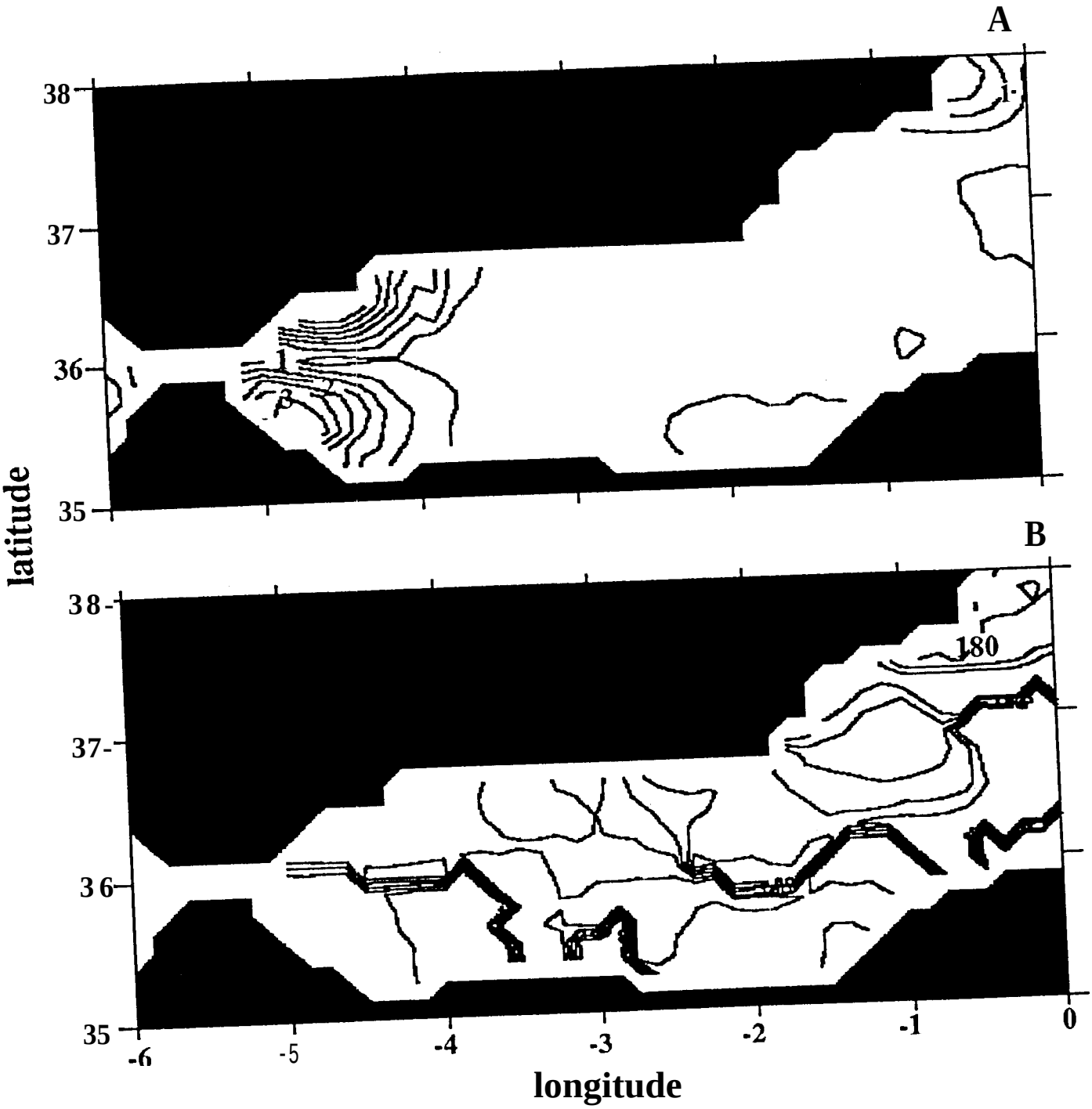
A
B
38
37
36
35
38
37
36
35
-6
-5
-4
-3
-2
-1
0
180
latitude
longitude

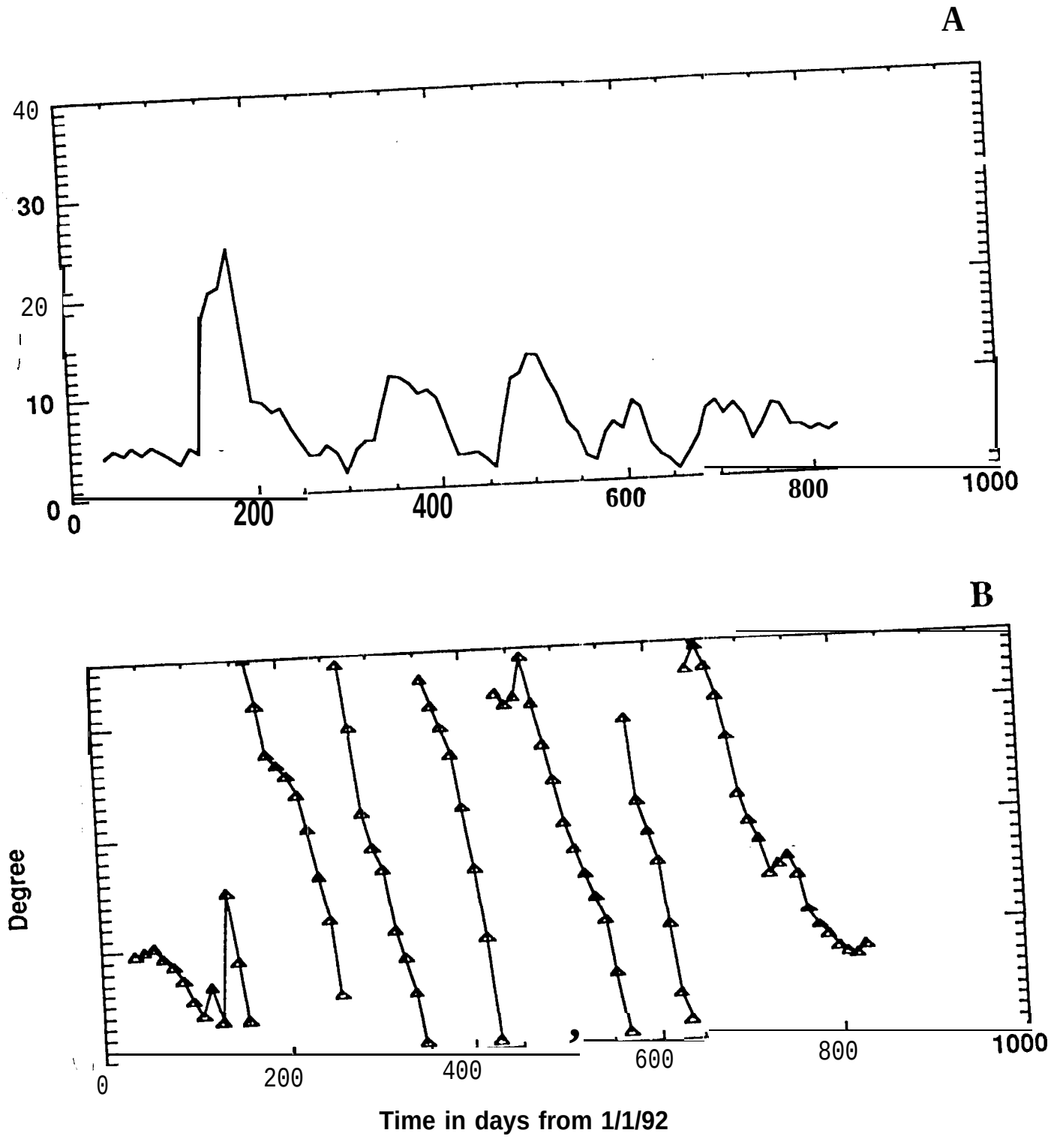
A
40
30
20
10
0
0
200
400
600
800
1000
B
Degree
0
200
400
600
800
1000
Time in days from 1/1/92

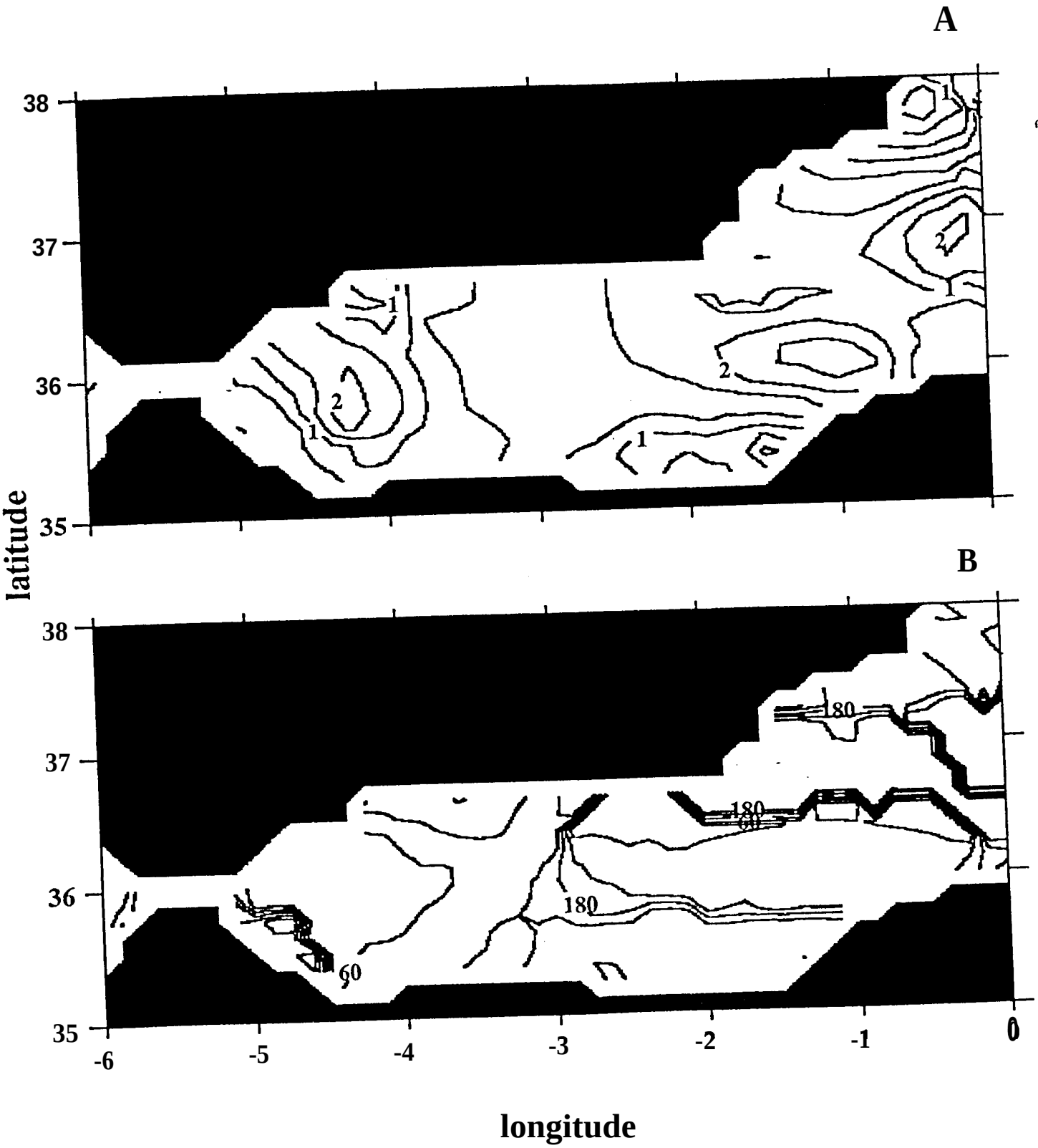
A
B
38
37
36
35
latitude
1
2
180
60
-6
-5
-4
-3
-2
-1
0
longitude

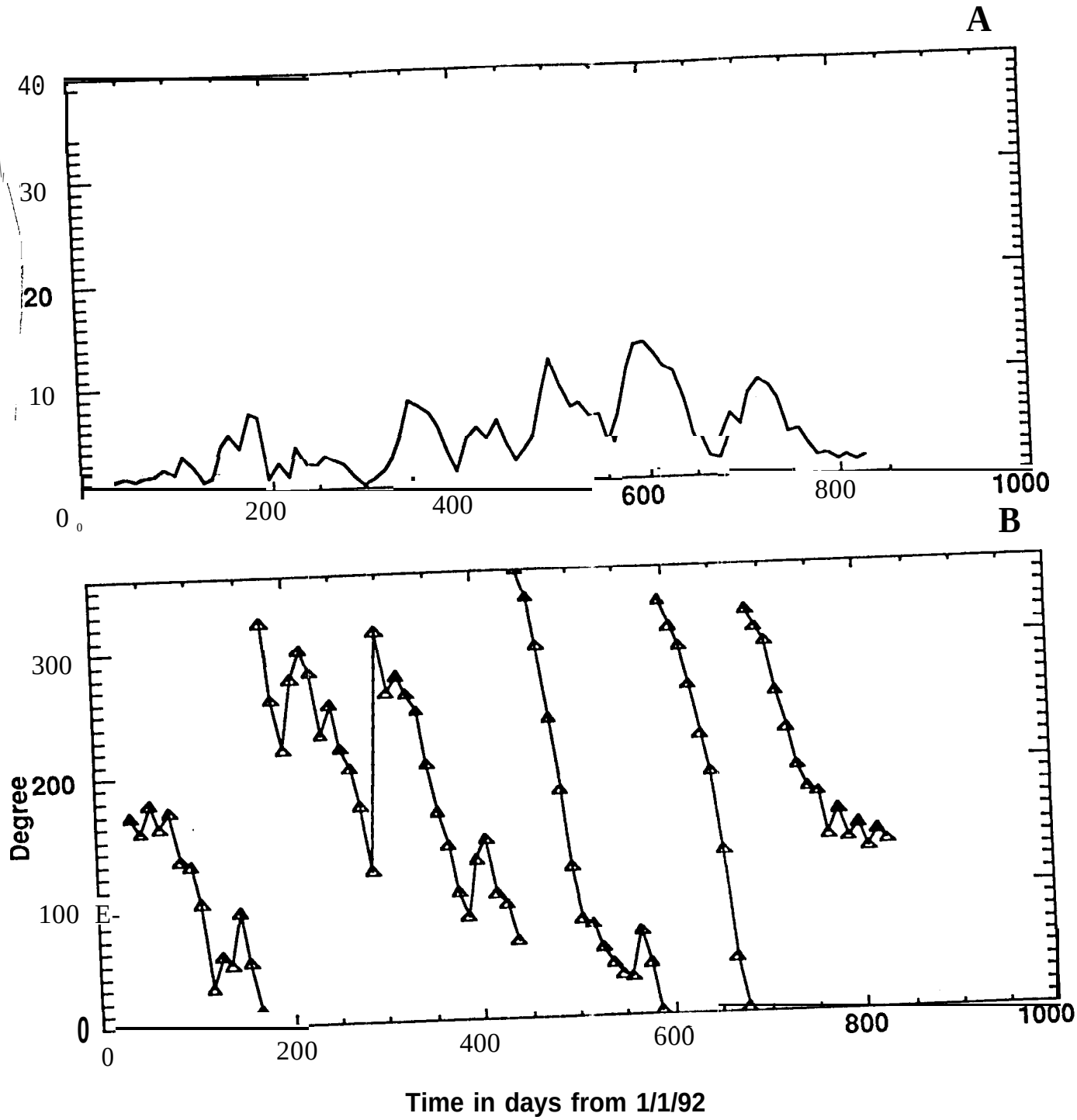
A
40
30
20
10
0
200
400
600
800
1000
B
300
200
100
0
Degree
0
200
400
600
800
1000
Time in days from 1/1/92

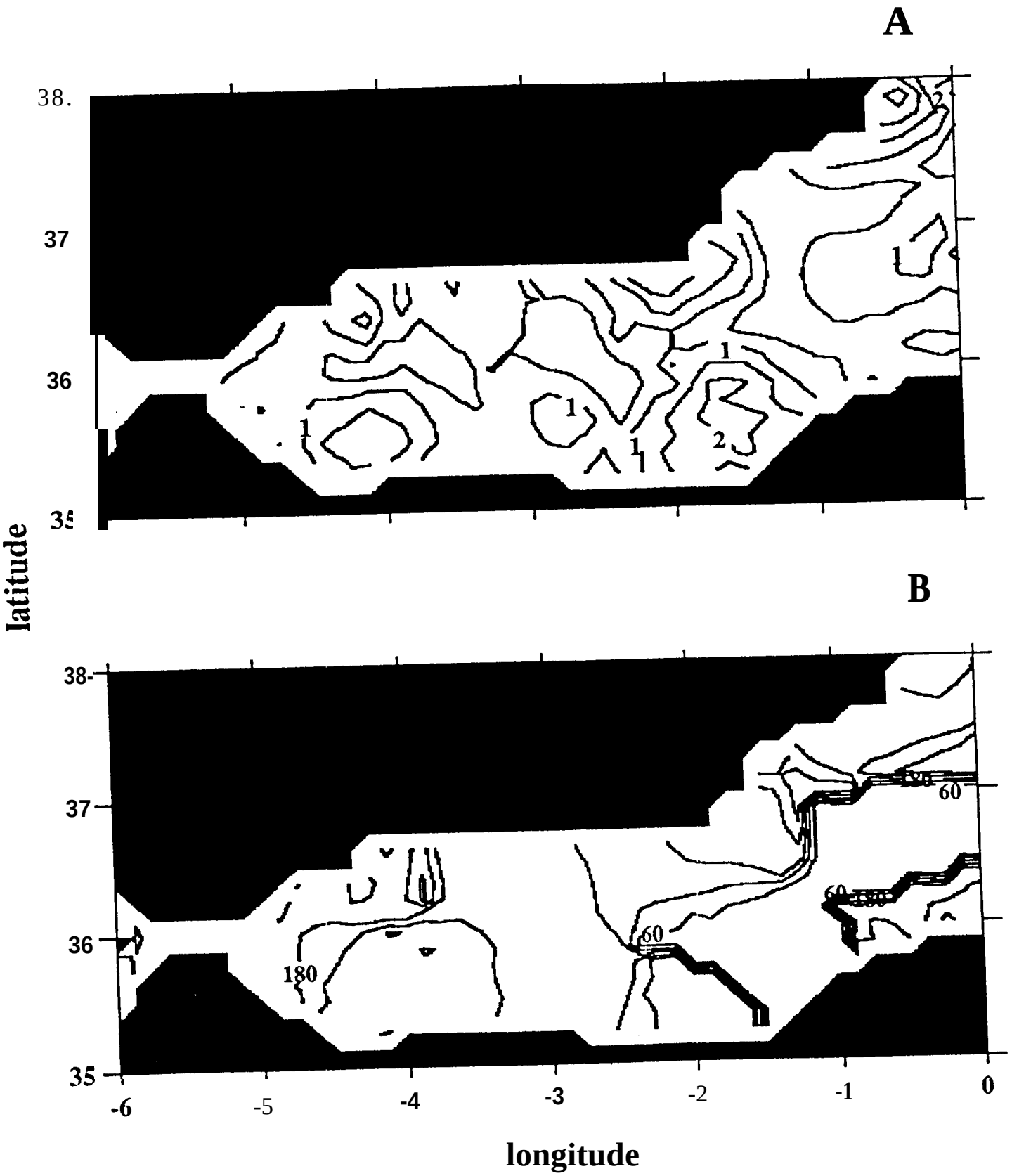
A
38.
37
36
35
2
1
1
1
1
1
2
B
38
37
36
35
-6
-5
-4
-3
-2
-1
0
60
60
60
180
180
latitude
longitude

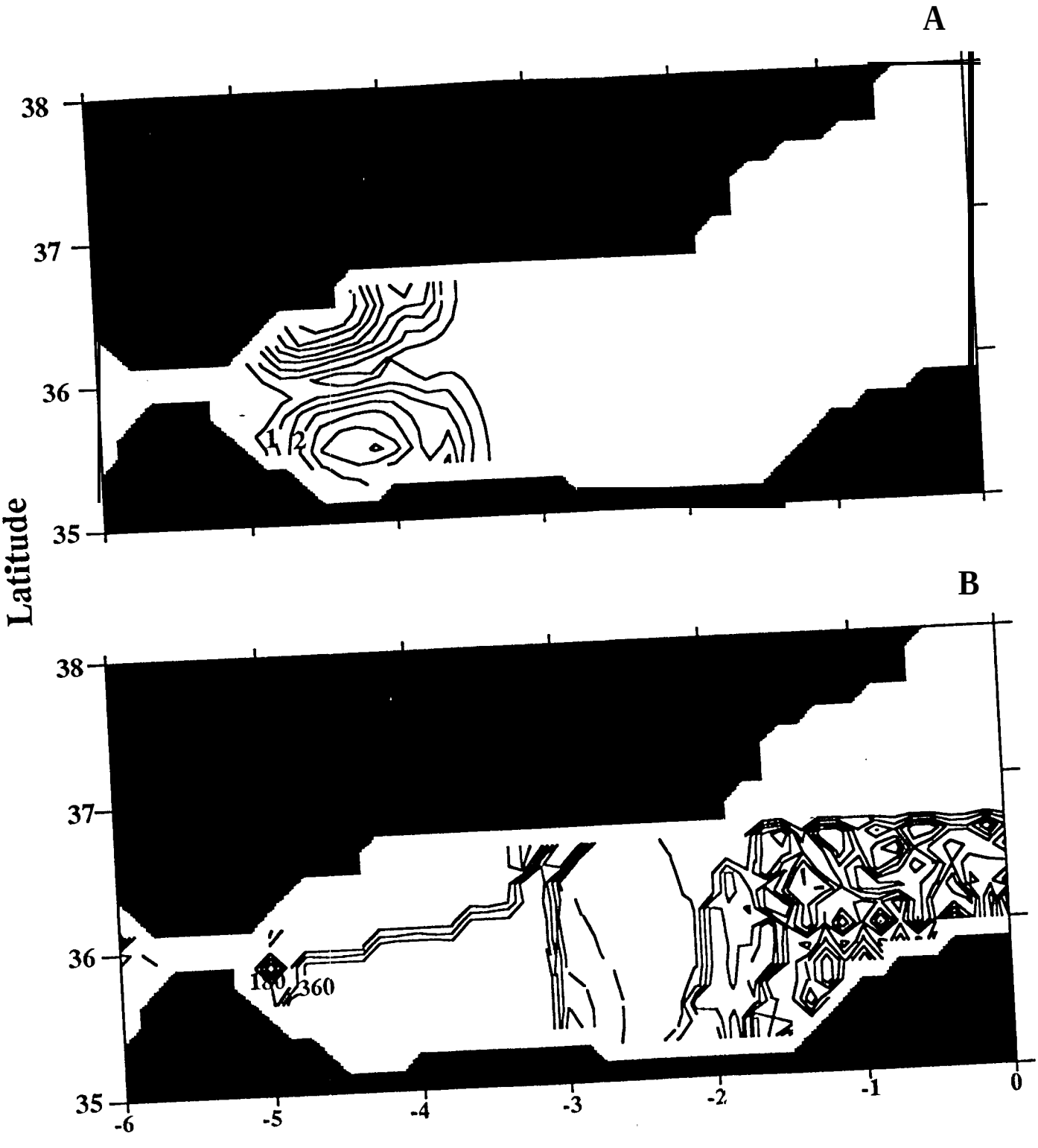
A
B
38
37
36
35
Latitude
1
2
4
180
360
-6
-5
-4
-3
-2
-1
0
Longitude